Nonlinear propagation of light in structured media: Generalized unidirectional pulse propagation equations

J. Andreasen[1] and M. Kolesik[1,2]
[1]*College of Optical Sciences, University of Arizona, Tucson, Arizona 85721, USA*
[2]*Department of Physics, Constantine the Philosopher University, Nitra, Slovakia*
(Received 22 June 2012; revised manuscript received 11 September 2012; published 27 September 2012)

Unidirectional pulse propagation equations [UPPE, Phys. Rev. E **70**, 036604 (2004)] have provided a theoretical underpinning for computer-aided investigations into dynamics of high-power ultrashort laser pulses and have been successfully utilized for almost a decade. Unfortunately, they are restricted to applications in bulk media or, with additional approximations, to simple waveguide geometries in which only a few guided modes can approximate the propagating waveform. The purpose of this work is to generalize the directional pulse propagation equations to structures characterized by strong refractive index differences and material interfaces. We also outline a numerical solution framework that draws on the combination of the bulk-media UPPE method with single-frequency beam-propagation techniques.

DOI: 10.1103/PhysRevE.86.036706 PACS number(s): 02.60.−x, 42.25.Bs, 42.65.Re, 42.65.Jx

I. INTRODUCTION

Computer simulations in the field of nonlinear optics have been playing an important role in understanding ever more extreme regimes in light-matter interactions. Dynamics of ultrashort, high-power laser pulses is one particular field, which motivated significant effort and concomitant progress in numerical methods designed for optics at femtosecond time scales. One can say that optical filamentation played the role of a catalyst for the development of a number of pulse propagation models, which made detailed studies of extremely nonlinear regimes a possibility. However, the most accurate pulse propagation models remain restricted to bulk media, both gaseous and condensed, while waveguiding structures have to be treated with more significant approximations.

The purpose of this paper is to put forward a theoretical framework, which will allow the implementation of simulators capable of handling pulse propagation regimes characterized by the following four attributes:

(A) structures with strong refractive index contrasts;

(B) directional long-distance wave propagation;

(C) strong waveform reshaping, both in time and space;

(D) extreme spectral dynamics, with resulting spectra often encompassing more than an octave in frequency.

This combination is rather difficult to handle numerically. For example, there exists a wealth of work (e.g., [1–5]) utilizing the beam propagation method (BPM), which is designed for regimes A and B, and can incorporate certain weak nonlinearities [6], but are restricted to narrow spectral regimes. Time-domain beam propagation methods have been developed (e.g., [7,8]), though they concentrate mainly on linear regimes. Direct Maxwell's equations solvers [9–11] are well suited to regimes A, C, and D, but are prohibitively expensive for simulating long-distance pulse propagation. Simulators based on the unidirectional pulse propagation equation (UPPE) [12,13] and other types of one-way propagation equations [14–23] can cope with attributes B, C, and D, but require additional approximations to simulate waveguiding structures, such as hollow-slab leaky waveguides [24] or nonlinear nanowaveguides [25–27]. In other words, methods suitable for the combination A + B + C + D have yet to be developed.

In this paper, we present a step in this direction and describe a generalization of the UPPE, which can be applied to nonlinear structured media with strong differences between refractive indices of the constituent materials. Rather than assuming unidirectional propagation from the outset, we depart from the wave equations and derive an auxiliary evolution system. This is used to find projection operators that extract forward and backward propagating components of the field from an arbitrary optical field waveform. These operators transform the auxiliary system into a coupled forward-backward pulse evolution system that is exact and accounts for structured media. Only then is the unidirectional propagation approximation applied, which maintains important terms otherwise lost if the approximation is made from the beginning—a similar approach as that of Kinsler and co-workers [22,23,28,29].

The key to the approach we present is that the pulse evolution equations are cast in a form which makes it possible to combine proven numerical methods. More specifically, nonlinear interactions can be treated by ordinary differential equation (ODE) libraries, the same way it has been done with UPPE-based simulators [30]; the linear propagator can be treated by tapping the rich knowledge base of BPM, and in particular the techniques developed for wide-angle BPM (WA-BPM) (see Refs. [31,32] for early formulation, and Refs. [33,34] for examples of various Padé approximated propagators).

The remainder of this paper is organized as follows. First, in Sec. II, we give a brief summary of the UPPE model. In Sec. III, this model is generalized and a coupled forward-backward pulse evolution system is derived. A unidirectional propagation approximation is applied and the resulting equation transformed into a form analogous to a bulk-medium UPPE. Considering a homogeneous medium finds the generalized equation reduces back to UPPE. Section IV outlines a strategy for a numerical solution of the generalized system and Sec. V presents illustrative simulation results for a capillary waveguide system. We summarize and discuss future directions in Sec. VI.

II. UNIDIRECTIONAL PULSE PROPAGATION EQUATIONS: SUMMARY

The main purpose of this paper is to generalize the UPPE framework. For the reader's convenience and ease of reference, we briefly summarize the corresponding equations.

In a homogeneous medium characterized by a dielectric permittivity $\epsilon(\omega)$, a pair of coupled UPPEs are exact [13,35] and can be written in the form

$$\partial_z \vec{E}_+^{\perp}(k_\perp,\omega,z) = +ik_z \vec{E}_+^{\perp}(k_\perp,\omega,z) + \sum_{s=1,2} \vec{e}_s^{\perp}\vec{e}_s \cdot\left[\frac{i\omega^2}{2\epsilon_0 c^2 k_z}\vec{P}(k_\perp,\omega,z) - \frac{\omega}{2\epsilon_0 c^2 k_z}\vec{J}(k_\perp,\omega,z)\right], \tag{1}$$

$$\partial_z \vec{E}_-^{\perp}(k_\perp,\omega,z) = -ik_z \vec{E}_-^{\perp}(k_\perp,\omega,z) - \sum_{s=1,2} \vec{e}_s^{\perp}\vec{e}_s \cdot\left[\frac{i\omega^2}{2\epsilon_0 c^2 k_z}\vec{P}(k_\perp,\omega,z) - \frac{\omega}{2\epsilon_0 c^2 k_z}\vec{J}(k_\perp,\omega,z)\right]. \tag{2}$$

These equations describe the evolution of $\vec{E}_\pm^{\perp}(k_\perp,\omega,z)$, which are the spectral (Fourier) representation of the electric field. $k_\perp = \{k_x,k_y,0\}$ are the transverse wave numbers and k_z is the z component of the wave vector,

$$\vec{k} = \left\{k_x,k_y,k_z \equiv \sqrt{\omega^2\epsilon(\omega)/c^2 - k_x^2 - k_y^2}\right\}, \tag{3}$$

which satisfies the dispersion relation $k^2 = \omega^2 n^2(\omega)/c^2$. The two polarization vectors $\vec{e}_s(k_\perp,\omega)$ are orthogonal to $\vec{k}$ and to each other, but otherwise can be chosen freely. The superscript $\perp$ denotes the transverse part (i.e., x,y) of the corresponding vector. Equations (1) and (2) are mutually coupled through the nonlinear medium polarization $\vec{P}(k_\perp,\omega,z)$ and current density $\vec{J}(k_\perp,\omega,z)$. These responses are functionals of the electric field. They are normally specified in the real-space and -time representation:

$$\vec{P}(r_\perp,t) = \vec{P}(\{\vec{E}(x,y,t)\}) \ , \ \vec{J}(r_\perp,t) = \vec{J}(\{\vec{E}(x,y,t)\}).$$

It has to be emphasized that the system of Eqs. (1) and (2) is exact and together with the $\vec{\nabla}\cdot\vec{D}$ equation (which can be used to obtain the z component of the field if needed) is equivalent to Maxwell's equations. However, as with direct Maxwell's equations solvers, it would be difficult to solve in its entirety, i.e., including forward and backward propagating waves. In practice, the unidirectional propagation approximation is assumed, and the medium response is calculated solely from the forward propagating waveform:

$$\vec{P}(\vec{E}),\vec{J}(\vec{E}) \rightarrow \vec{P}(\vec{E}_+),\vec{J}(\vec{E}_+). \tag{4}$$

Under this approximation the system reduces to a single UPPE, Eq. (1). For details of the numerical solution, the reader is referred to Ref. [30]. Here we only point out that the native representation suitable for numerical implementation relies on spectral amplitudes $\vec{A}_{s,+}(k_\perp,\omega,z)$, which only change with z due to nonlinear interactions with the medium. They are related to the electric field through the linear propagator $e^{ik_z(k_x,k_y,\omega)z}$:

$$\vec{E}_+^{\perp}(k_\perp,\omega,z) = \sum_{s=1,2} \vec{e}_s^{\perp}\vec{A}_{s,+}(k_\perp,\omega,z)e^{ik_z(k_x,k_y,\omega)z}. \tag{5}$$

The corresponding UPPE equation,

$$\partial_z A_{s,+}(k_\perp,\omega,z) = \frac{\omega e^{-ik_z z}}{2\epsilon_0 c^2 k_z} \vec{e}_s \cdot [i\omega\vec{P}(k_\perp,\omega,E_+(z)) - \vec{J}(k_\perp,\omega,E_+(z))], \tag{6}$$

constitutes a large system of ODEs. This is the representation in which it is solved numerically. Because the medium response is calculated in the real-time representation at each spatial point, spectral transforms in both directions have to be invoked multiple times when the right-hand side of the ODE system is evaluated.

The main limitation of the UPPE approach is that it is restricted to homogeneous media. Weakly guiding structures can be included as part of the polarization response, but geometries with strong material contrasts and interfaces cannot be efficiently simulated. Reference [13] shows a derivation of the UPPE system for waveguiding structures, but its implementation requires knowledge of the full system of electromagnetic modal fields, which is impractical to obtain even for geometries that admit exact solutions. Therefore, waveguiding scenarios can only be simulated under additional assumptions, which require that the fields can be described as a superposition of a few guided or leaky modes of the structure, whatever field configurations evolve.

The practical limitation of the UPPE, and in fact of all other unidirectional pulse propagation methods, originates in the identification of the forward and backward propagating waves resting on the usage of a reference homogeneous medium. To elucidate this, let us consider the following example. Let $\epsilon(\omega)$ represent a chosen homogeneous background, and let $\chi(\vec{r}_\perp,\omega)$ be such that $\epsilon + \chi(r_\perp)$ gives the actual permittivity of the structure. The variable part $\chi(r_\perp)$ can be treated within the polarization term of Eq. (6), $P(r) = \epsilon_0\chi(r_\perp)E_+(r_\perp)$. Now note that even if χ is constant throughout space, the propagation constant of a plane wave predicted by Eq. (6), i.e., $k_z(\omega,k_\perp) + \chi\omega^2/[2c^2k_z(\omega,k_\perp)]$, is only a second-order Taylor approximation to the exact plane-wave propagation constant $\sqrt{\omega^2[\epsilon(\omega)+\chi(\omega)]/c^2 - k_\perp^2}$. On the other hand, it is straightforward to show that if we retained both coupled UPPEs (1) and (2), the resulting propagation constant would be exact, independently of the choice of the reference $\epsilon(\omega)$. We thus see that if $\chi(r_\perp)$ varies in space, no matter how we select the reference medium $\epsilon(\omega)$, even the linear problem is not solved exactly by a single UPPE. This means that if we wish to use the unidirectional approximation for nonlinear interactions, we must find a way to marry it with an exact propagation description in the linear limit. This in turn implies that no part of the refractive index variation in space should be included in the polarization term of the propagation equation.

III. DIRECTIONAL PULSE PROPAGATION EQUATIONS

In this section, we generalize unidirectional pulse propagation equations to situations with material interfaces parallel to the propagation direction z and with strong refractive index

differences between materials that comprise the structure. Central to this task will be the ability to extract the true forward and backward propagating components of the total electromagnetic field. The main deviation from the method described above is that the pulse propagator native representation will be mixed. We will retain the spectral representation of the frequency (time) dimension, but will use the real space representation for the transverse spatial dimensions x,y. This "mixed representation" approach is often applied, e.g., to simulations of femtosecond filaments because it allows the use of nonhomogeneous grids and better boundary conditions [30]. In our case, the main rationale for real-space representation in the transverse cross section is the need to accommodate material interfaces.

A. Model of a nonlinear, structured medium

Consider a nonmagnetic, isotropic dispersive medium, with the dielectric permittivity $\epsilon(x,y,\omega)$, which only depends on coordinates x and y and angular frequency ω. We assume there are no free charges or currents. The constitutive relation for all media will be written in a form using polarization to account for all properties except the linear $\epsilon(\omega)$,

$$\mathbf{P} = \mathbf{P}(x,y,\{\mathbf{E}(x,y,t)\}). \tag{7}$$

We assume that an algorithm is given that computes polarization from a given history of the electric field vector $\mathbf{E}(x,y,t)$ at a specified point $[x,y]$. The first two arguments of $\mathbf{P}$ are meant to indicate that this algorithm can depend, through the medium properties, on the transverse location $[x,y]$ but not on the longitudinal coordinate z. The concrete functional form of $\mathbf{P}$ is unimportant for the present purposes, but for a specific example, the reader can think of the instantaneous optical Kerr effect in which the local index of refraction changes proportionally to the square of the electric field vector. As the medium is isotropic, the polarization direction follows that of $\mathbf{E}$:

$$\mathbf{P}_{Kerr}(x,y,\{\mathbf{E}(x,y,t)\}) = 2\epsilon_0\bar{n}_2(x,y)\left(E_x^2+E_y^2+E_z^2\right)\mathbf{E}. \tag{8}$$

Here, $\bar{n}_2(x,y)$ stands for the nonlinear index, which as it indicates, may depend on location. Other models of light-matter interactions that have been used in simulations are described in articles on filamentation [36,37] and Ref. [30] shows methods for their numerical implementation.

To keep notation simple, we will not use current density explicitly. In general, nonlinear interactions with the medium can be equivalently formulated either in the polarization or current density language, so this means no loss of generality. In numerical simulations, using both current and polarization may actually be convenient, and it only requires trivial extension of our results.

B. Fields in terms of analytic signals

In numerical simulations, it is often easier to work with the so-called analytic signals of the electric field. They are commonly used to represent real-valued quantities in terms of complex-valued representations. Here we use analytic signals to represent all real quantities $(\mathbf{E}(t),\mathbf{P}(t))$. For example, the electric field is obtained as a real part of its analytic signal:

$$\mathbf{E} = \mathrm{Re}\{\vec{E}(x,y,z,t)\}, \tag{9}$$

which has its spectrum restricted to positive frequencies:

$$\vec{E}(x,y,z,t) = \int_0^\infty d\omega \vec{E}(x,y,z,\omega)e^{-i\omega t}. \tag{10}$$

Here, and in what follows, we will distinguish between temporal and spectral representations of functions through their respective arguments t and ω. Because the only time we need the representation of the electric field in the time domain is when we compute the nonlinear medium response (i.e., polarization), we will work mostly in the spectral representation.

C. Derivation of directional pulse propagation equations

Our departure point is the wave equation for the electric field, accompanied by a constraint in the form of the divergence equation,

$$\vec{\nabla}\vec{\nabla}\cdot\vec{E} - \nabla^2\vec{E} = \frac{\omega^2}{c^2}\left(\epsilon\vec{E}+\frac{1}{\epsilon_0}\vec{P}\right),\ \vec{\nabla}\cdot\vec{D}=0. \tag{11}$$

While we have assumed no free charges and currents, high intensities can lead to medium ionization and subsequently to electrons drifting away from their parent ions. However, our treatment aims to describe femtosecond pulses. On such a short time scale we can safely assume that even when ionization occurs, the positive and negative charges do not have enough time to separate, and the average local charge remains zero. Therefore, using the divergence equation,

$$\vec{\nabla}\cdot\vec{D} = \epsilon_0\epsilon\vec{\nabla}\cdot\vec{E} + \epsilon_0\vec{E}\cdot\vec{\nabla}\epsilon + \vec{\nabla}\cdot\vec{P} = 0, \tag{12}$$

$\vec{\nabla}\cdot\vec{E}$ can be expressed in terms of the nonlinear polarization divergence and transverse electric field components as follows:

$$-\vec{\nabla}\cdot\vec{E} = \frac{1}{\epsilon}\vec{E}_\perp\cdot\vec{\nabla}_\perp\epsilon + \frac{1}{\epsilon_0\epsilon}\vec{\nabla}\cdot\vec{P}. \tag{13}$$

The transverse (x,y) part of the wave equation is thus rewritten to separate the linear and nonlinear terms,

$$-\partial_{zz}\vec{E}_\perp = \hat{L}\vec{E}_\perp + \hat{N}_\perp[\vec{E}]. \tag{14}$$

Here, the linear operator $\hat{L}$ is related to the corresponding Helmholtz equation (for a fixed angular frequency). It acts only on the transverse electric field vector,

$$\hat{L}\vec{E}_\perp \equiv \frac{\omega^2}{c^2}\epsilon(r_\perp,\omega)\vec{E}_\perp + \Delta_\perp\vec{E}_\perp + \vec{\nabla}\frac{1}{\epsilon}\vec{E}_\perp\cdot\vec{\nabla}_\perp\epsilon. \tag{15}$$

The nonlinear operator $\hat{N}$ acts on $\vec{E}_\perp$, but in general, also depends on the E_z component

$$\hat{N}[\vec{E}] \equiv \frac{\omega^2}{\epsilon_0 c^2}\vec{P}(\vec{E}) + \vec{\nabla}\frac{1}{\epsilon_0\epsilon}\vec{\nabla}\cdot\vec{P}(\vec{E}). \tag{16}$$

We will address how to obtain E_z later. For now, let us assume that it can be calculated once $E_{x,y}$ are known. To obtain propagation equations for $\vec{E}_\perp(z,x,y,\omega)$, we first introduce auxiliary field amplitudes, effectively doubling the number of variables used to describe the electric field:

$$E_i(z,x,y,\omega) = E_i^+(z,x,y,\omega) + E_i^-(z,x,y,\omega), \tag{17}$$

with

$$E_i^+ = A_i^+(z,x,y,\omega)e^{+i\zeta z},$$
$$E_i^- = A_i^-(z,x,y,\omega)e^{-i\zeta z}, \tag{18}$$

where $i = x,y$ and ζ stands for a parameter to be chosen freely. Clearly, since ζ appears in neither Maxwell's nor the wave equations, physical observables must not depend on the concrete choice of ζ, and this "gauge invariance" will become manifest when we arrive at our final result. We define ζ as a reference wave number to emphasize the fact that it has no physical meaning by itself.

It is also important to keep in mind that the positive and negative wave-number parts $E_i^\pm$ of the field are, in general, not the forward and backward propagating portions of the total waveform. So far we have not restricted how fast $A_i^\pm$ can change with z. In principle, they could evolve so fast that their variation would completely override the exponential factors $e^{\pm i\zeta z}$ accompanying them. That is why both $E_i^\pm$ can contribute to waves propagating in the positive and negative z direction (see Ref. [29] for how this occurs). These auxiliary amplitudes will help us to construct a unidirectional approximation in a consistent way—but before we can do this, we must first account for both (or all) directions of propagation (e.g., see Ref. [22]).

By representing a single function $E_i(z,x,y,\omega)$ as a combination of two functions $E_i^\pm(z,x,y,\omega)$, we have added artificial degrees of freedom. These will be taken back by requiring that $E_i^\pm$ satisfy a relation of our choice. Concretely, we impose an additional constraint in the form

$$e^{+i\zeta z}\partial_z A_i^+(z,x,y,\omega) + e^{-i\zeta z}\partial_z A_i^-(z,x,y,\omega) = 0. \tag{19}$$

The rationale behind this constraint is exactly the same as in the variation of constants method for differential equations. Namely, this representation eliminates the second derivatives when one evaluates $\partial_{zz}E$. Because of the constraint, the first derivative simplifies to

$$\partial_z E_i = i\zeta(E_i^+ - E_i^-) \tag{20}$$

and the second derivative to

$$\partial_{zz}E_i = -\zeta^2 E_i + i\zeta e^{+i\zeta z}\partial_z A_i^+ - i\zeta e^{-i\zeta z}\partial_z A_i^-. \tag{21}$$

Using this in the wave equation (14) together with the constraint of Eq. (19), we obtain the evolution equations for the auxiliary amplitudes $A^\pm$:

$$\partial_z A_i^\pm = \frac{\pm i}{2\zeta}e^{\mp i\zeta z}[(\hat{L}-\zeta^2)\vec{E}_\perp + \hat{N}_\perp[\vec{E}]]. \tag{22}$$

To evaluate the right hand side of this system, $\vec{E}_\perp$ is expressed in terms of $A_i^\pm$, and E_z is subsequently obtained from the z component of the wave equation. Using Eq. (20), the latter can be written as follows:

$$i\zeta\partial_x(E_x^+ - E_x^-) + i\zeta\partial_y(E_y^+ - E_y^-) - \frac{\omega^2}{c^2\epsilon_0}P_z(\vec{E})$$
$$= \partial_{xx}E_z + \partial_{yy}E_z + \frac{\omega^2\epsilon}{c^2}E_z. \tag{23}$$

If not for nonlinearity, this is an inhomogeneous Helmholtz equation that determines E_z in terms of the transverse field components. The part of the polarization component P_z which is nonlinear in E_z is usually very small and therefore normally neglected. Should one not be satisfied with such an approximation, the above equation can be solved by iteration. For example, in Kerr media for intensities typical of femtosecond filaments, a single iteration already gives an accurate result.

The next step consists in identifying the parts of the electric field waveform, which propagate in the positive and negative directions along the z axis. The resulting equations become more intuitive when expressed in terms of auxiliary E fields:

$$\partial_z E_i^+ = +i\zeta E_i^+ + \frac{i}{2\zeta}[(\hat{L}-\zeta^2)\vec{E}_\perp + \hat{N}_\perp[\vec{E}]], \tag{24}$$

$$\partial_z E_i^- = -i\zeta E_i^- - \frac{i}{2\zeta}[(\hat{L}-\zeta^2)\vec{E}_\perp + \hat{N}_\perp[\vec{E}]]. \tag{25}$$

This system, completed by Eq. (23), is equivalent to the wave equation with the divergence constraint, and can be solved in principle. However, in this form, it poses two problems. First, in general, it would require very short propagation steps in order to resolve both the forward and backward propagating waves. Second, the physical input conditions for simulations are normally given such that the problem to solve is a boundary value problem rather than an initial value problem. The latter point becomes evident when we realize that it is only the forward-propagating field component that is specified at $z = 0$ (e.g., at the laser output). The second condition is that the backward propagating field is zero at $z \to \infty$ (i.e., at the far end of a laboratory). Such a boundary value problem would be rather difficult to solve. Fortunately, in many cases the backward propagating wave can be neglected. We shall therefore derive the beam propagation equations that account for such a situation, but in the process shall identify the forward and backward propagating fields (and see that they are, in general, different from $E^\pm$).

In matrix notation, the propagation equations read

$$\partial_z\begin{pmatrix}\vec{E}_\perp^+\\ \vec{E}_\perp^-\end{pmatrix} = i\begin{pmatrix}\zeta + \frac{\hat{L}-\zeta^2}{2\zeta} & +\frac{\hat{L}-\zeta^2}{2\zeta}\\ -\frac{\hat{L}-\zeta^2}{2\zeta} & -\zeta - \frac{\hat{L}-\zeta^2}{2\zeta}\end{pmatrix}\begin{pmatrix}\vec{E}_\perp^+\\ \vec{E}_\perp^-\end{pmatrix}$$
$$+\frac{i}{2\zeta}\begin{pmatrix}+\hat{N}_\perp[\vec{E}]\\ -\hat{N}_\perp[\vec{E}]\end{pmatrix}. \tag{26}$$

Having separated the linear and nonlinear part of the evolution operator, we are in the position to determine the forward and backward propagating parts of the field. This division will be defined with respect to the linear system. In a spirit similar to Ref. [12], two projector operators can be constructed from the Helmholtz operator $\hat{L}$ and its square root $\hat{L}^{1/2}$:

$$\mathcal{P}_F \equiv \frac{\hat{L}^{-1/2}}{4\zeta}\begin{pmatrix}+(\zeta+\hat{L}^{1/2})^2 & +(\hat{L}-\zeta^2)\\ -(\hat{L}-\zeta^2) & -(\zeta-\hat{L}^{1/2})^2\end{pmatrix}, \tag{27}$$

$$\mathcal{P}_B \equiv \frac{\hat{L}^{-1/2}}{4\zeta}\begin{pmatrix}-(\zeta-\hat{L}^{1/2})^2 & -(\hat{L}-\zeta^2)\\ +(\hat{L}-\zeta^2) & +(\zeta+\hat{L}^{1/2})^2\end{pmatrix}. \tag{28}$$

It is straightforward to show that these operators have the expected properties of projectors, in particular they are idempotent,

$$\mathcal{P}_F^2 = \mathcal{P}_F, \quad \mathcal{P}_B^2 = \mathcal{P}_B, \tag{29}$$

and they constitute a unity decomposition,

$$\mathcal{P}_F + \mathcal{P}_B = 1, \quad \mathcal{P}_F\mathcal{P}_B = \mathcal{P}_B\mathcal{P}_F = 0. \tag{30}$$

These projectors also commute with the linear evolution operator in Eq. (26), and direct calculation shows that their eigenvectors have propagation constants corresponding to forward and backward modes propagating in the linear system. Thus, we can use these projectors to obtain the true forward and backward propagating field components. If the total field is given in terms of the auxiliary amplitudes $\vec{E}_\perp^{\pm}$, then the forward portion of the wave is obtained as

$$\begin{aligned} E_F &= (1\ \ 1)\mathcal{P}_F \begin{pmatrix} \vec{E}_\perp^{+} \\ \vec{E}_\perp^{-} \end{pmatrix} \\ &= \frac{1}{2}[(\vec{E}_\perp^{+} + \vec{E}_\perp^{-}) + \hat{L}^{-1/2}\zeta(\vec{E}_\perp^{+} - \vec{E}_\perp^{-})]. \end{aligned} \tag{31}$$

This expression contains the reference wave number, which might suggest that it depends on our artificial split of the field in Eq. (17). However, because of Eq. (20), the above expression reduces to

$$E_F = \frac{1}{2}\vec{E}_\perp - \frac{i}{2}\hat{L}^{-1/2}\partial_z\vec{E}_\perp \tag{32}$$

and the backward propagating component is obtained as

$$E_B = \frac{1}{2}\vec{E}_\perp + \frac{i}{2}\hat{L}^{-1/2}\partial_z\vec{E}_\perp. \tag{33}$$

As they must be, these forward and backward amplitudes are independent of the reference wave number. Our aim is to express the pulse evolution equations in terms of these directional fields. Because the projector operators are z independent, the simplest way is to apply them directly to the propagation equations. In other words, we need to compute

$$\partial_z E_\perp^F = (1\ \ 1)\mathcal{P}_F \begin{pmatrix} \partial_z\vec{E}_\perp^{+} \\ \partial_z\vec{E}_\perp^{-} \end{pmatrix}, \tag{34}$$

$$\partial_z E_\perp^B = (1\ \ 1)\mathcal{P}_B \begin{pmatrix} \partial_z\vec{E}_\perp^{+} \\ \partial_z\vec{E}_\perp^{-} \end{pmatrix}. \tag{35}$$

Inserting the right hand side from Eq. (26) and using the projector properties of Eqs. (29) and (30), we obtain a pair of coupled equations for the forward and backward fields,

$$\begin{aligned} \partial_z E_\perp^F &= +i\sqrt{\hat{L}}E_\perp^F + \frac{i}{2\sqrt{\hat{L}}}\hat{N}_\perp[E^F + E^B], \\ \partial_z E_\perp^B &= -i\sqrt{\hat{L}}E_\perp^B - \frac{i}{2\sqrt{\hat{L}}}\hat{N}_\perp[E^F + E^B]. \end{aligned} \tag{36}$$

This is a generalization of the coupled pair of unidirectional pulse propagation equations (1) and (2). We show later that in a homogeneous medium, for which we have an explicit expression for the square root of the Helmholtz operator, these equations reduce to UPPEs as they should.

Similar to the case for bulk media, Eq. (36) is not the best for numerical implementation. We transform this system into a form analogous to that of bulk UPPE (6) such that we can adopt the same numerical solution strategy. Toward this purpose, we use amplitudes which will exhibit evolution only if some nonlinearity is present:

$$E_\perp^F = e^{+i\sqrt{\hat{L}}z}A_\perp^F(z), \quad E_\perp^B = e^{-i\sqrt{\hat{L}}z}A_\perp^B(z). \tag{37}$$

In this representation, Eq. (36) reads

$$\begin{aligned} \partial_z A_\perp^F &= \frac{+i}{2\sqrt{\hat{L}}}e^{-i\sqrt{\hat{L}}z}\hat{N}_\perp[e^{+i\sqrt{\hat{L}}z}A^F + e^{-i\sqrt{\hat{L}}z}A^B], \\ \partial_z A_\perp^B &= \frac{-i}{2\sqrt{\hat{L}}}e^{+i\sqrt{\hat{L}}z}\hat{N}_\perp[e^{+i\sqrt{\hat{L}}z}A^F + e^{-i\sqrt{\hat{L}}z}A^B]. \end{aligned} \tag{38}$$

This shows explicitly that the forward and backward propagating waves are mutually coupled in the nonlinear terms. It is obvious that for strong nonlinearity, our forward-backward projection loses its intended meaning, because it can renormalize and couple waves propagating in both main directions [28]. Thus, we arrive at a point where we must adopt an approximation which will allow us to reduce the full system to a single unidirectional equation.

D. Unidirectional propagation approximation

Our final step is to adopt the unidirectional approximation, where we assume that the nature and strength of nonlinearity is such that only negligible backward propagating fields are generated. Then, the nonlinear term can be approximated as

$$\hat{N}_\perp[e^{+i\sqrt{\hat{L}}z}A^F + e^{-i\sqrt{\hat{L}}z}A^B] \approx \hat{N}_\perp[e^{+i\sqrt{\hat{L}}z}A^F] \tag{39}$$

and the system can be restricted to only the forward-propagating field:

$$\partial_z A_\perp^F(r_\perp,\omega,z) = +\frac{i}{2\sqrt{\hat{L}}}e^{-i\sqrt{\hat{L}}z}\hat{N}_\perp[e^{+i\sqrt{\hat{L}}z}A^F]. \tag{40}$$

This is the sought-after generalization of the unidirectional pulse propagation equation. As expected, the structure of this system is completely analogous to the bulk UPPEs of Eq. (6), with the exception that the linear propagator is formally expressed in terms of a Helmholtz square root operator, instead of a plane-wave expansion. The most pronounced difference is that Eq. (40) is natively represented in the mixed representation. It retains the spectral treatment of the time dimension and with that, it preserves the ability to treat chromatic and nonlinear properties of the material exactly. On the other hand, the transverse dimensions are represented in real space, which is the natural choice for the implementation of the linear propagator in a structured medium with strong refractive index variations.

E. Special case: Reduction to UPPE in a homogeneous medium

Before going into how this pulse evolution equation can be solved numerically, let us illustrate how it reduces to the well-known bulk UPPE for a homogeneous medium. First, we recall that for a homogeneous medium, we know that plane waves are eigenfunctions of the Helmholtz operator $\hat{L}$ and that in the plane-wave representation, the linear propagator reduces to multiplication by a phase factor given by the propagation constant $k_z(\omega,k_\perp)$:

$$e^{-i\sqrt{\hat{L}}z} = e^{-ik_z(\omega,k_\perp)z}.$$

It is therefore sufficient to Fourier transform Eq. (40) from the (x,y) space to the transverse wave-number space (k_x,k_y) to obtain

$$\partial_z A_\perp^F(k_\perp,\omega,z) = +\frac{i}{2k_z}e^{-ik_z z}\hat{N}_\perp[e^{+ik_z z}A^F], \tag{41}$$

then using Eq. (37),

$$\partial_z E_\perp^F(k_\perp,\omega,z) = +ik_z E_\perp^F(k_\perp,\omega,z) + \frac{i}{2k_z}\hat{N}_\perp[E^F], \quad (42)$$

and express $\hat{N}$ in terms of polarization:

$$\partial_z E^F = ik_z E^F + \frac{i}{2k_z}\left[\frac{\omega^2}{\epsilon_0 c^2}\vec{P}(\vec{E}) - \frac{1}{\epsilon_0\epsilon}\vec{k}\vec{k}\cdot\vec{P}(\vec{E})\right]. \quad (43)$$

Only the transverse components in this equation constitute the evolution system, but in this full-vector form, it is easy to see that the operator acting on the polarization term produces the transverse part of the nonlinear response, namely

$$\left[\frac{\omega^2}{\epsilon_0 c^2}\vec{P}(\vec{E}) - \frac{1}{\epsilon_0\epsilon}\vec{k}\vec{k}\cdot\vec{P}(\vec{E})\right] = \frac{\omega^2}{\epsilon_0 c^2}\left[1 - \frac{\vec{k}\vec{k}\cdot}{k^2}\right]\vec{P}(\vec{E}). \quad (44)$$

The projector operator in the square brackets can be replaced by a sum over projectors on the polarization vectors $\vec{e}_s$,

$$\left[1 - \frac{\vec{k}\vec{k}\cdot}{k^2}\right] = \sum_s \vec{e}_s\vec{e}_s\cdot \quad (45)$$

Using this in Eq. (44) and inserting it into Eq. (43), we obtain

$$\partial_z E_\perp^F(z,\omega,k_\perp) = ik_z E_\perp^F + \frac{i\omega^2}{2\epsilon_0 c^2 k_z}\sum_s \vec{e}_s^{\perp}\vec{e}_s\cdot\vec{P}(\vec{E}), \quad (46)$$

which is identical to the homogeneous medium UPPE of Eq. (1) (with the current density term omitted). Thus, as it must, the generalized pulse propagation equation (40) passes this sanity check and reduces to the UPPE if the medium is homogeneous.

IV. NUMERICAL SOLUTION STRATEGY

In this section we sketch, in broad strokes, an approach for the numerical solution. It builds on the ODE-based method for solving UPPE systems and combines it with a wide-angle beam-propagation solver used to evaluate the linear propagator $\exp(i\hat{L}^{1/2}z)$.

The core of the pulse propagator of Eq. (40) is an ODE system, with z being the independent variable. The equation is evaluated at every transverse spatial location $r_\perp$ and frequency ω while being incremented along the propagation direction z. During a single ODE step, the right hand side of Eq. (40) has to be evaluated multiple times at different values of z which are subject to the choice of the specific ODE algorithm. Because the integration is normally executed with an adaptive integration step, one cannot determine beforehand at what specific z locations the term $[\exp(i\hat{L}^{1/2}z)A]$ needs to be computed—an algorithm is needed to evaluate the right hand side for *any* small value of z. For the ODE solver, we use the open source Gnu Scientific Library (GSL), but any implementation with the following capabilities can be chosen. One necessary feature of a suitable ODE library is a driver for adaptive step control, with a robust algorithm monitoring the accuracy of the numerical solution. Another necessity is that the library contains methods which do not require Jacobian evaluation, because such methods are not suitable for UPPE-like ODE systems [30]. We typically employ the Runge-Kutta-Fehlberg method, however, another useful ODE library feature is the capability to switch easily between different integration methods. Regarding its structure and method of solution as an ODE system, the generalized propagation equation does not differ from an ordinary UPPE. What is different is the implementation of the linear propagator.

Because the linear propagator is diagonal in angular frequency, this task is equivalent to a set of uncoupled beam-propagation problems. In other words, the action of $\exp(i\hat{L}^{1/2}z)A$ only requires one independent BPM-like update for each ω resolved in the simulation. This portion of the algorithm is therefore "embarrassingly parallel," with perfect balance and no interdependencies between calculations performed for different angular frequencies. There are many wide-angle BPM methods available, and any of them can be utilized, in principle. For instance, one can evaluate the linear propagator by a Padé approximant. Defining $\beta^2(\omega) \equiv \omega^2\epsilon(\omega)/c^2$, the dominant part of the Helmholtz operator, one writes

$$e^{i\sqrt{\hat{L}}\Delta z} = e^{i\beta\sqrt{1+\hat{X}}\Delta z} = \prod_k \frac{\hat{X}+a_k}{\hat{X}+b_k}. \quad (47)$$

The coefficients a_k, b_k depend on Δz and are chosen as to reproduce the Taylor expansion of the left hand side. For example,

$$\frac{4i + (i-\beta\Delta z)\hat{X}}{4i + (i+\beta\Delta z)\hat{X}}e^{i\beta\Delta z} \quad (48)$$

is second-order accurate in $\hat{X}$ with the error scaling as $\sim\beta\Delta z\hat{X}^3$. Various higher order approximations can be constructed in the same spirit. If the operator $\hat{X}$ acts in a nontrivial way along both spatial dimensions x,y, it is often further split into "one-dimensional" components so that the resulting matrices are band diagonal.

Similar techniques can be used to compute the inverse square root of $\hat{L}$ that acts on the nonlinear response term in Eq. (40). However, this operator can be approximated by $\hat{L}^{1/2} \approx \omega n(\omega)/c$, as is usually done in filamentation simulations [30]. This is sufficient unless the spatial profile of the nonlinear polarization becomes "focused" to wavelength scale.

With the linear propagator implemented as a "BPM-based plug-in," the solution proceeds in steps with two stages as follows:

(1) *Call the ODE solver*. One integration step is executed that updates the current $A(r_\perp,\omega,z)$ into the new $A(r_\perp,\omega,z+\Delta z)$. The ODE solver algorithm invokes computation of the right hand side of Eq. (40),

$$+\frac{i}{2\beta}e^{-i\sqrt{\hat{L}}\delta z}\hat{N}_\perp[e^{+i\sqrt{\hat{L}}\delta z}A^F],$$

which contains two applications of the linear propagator [e.g., Eq. (48)] for a substep $\pm\delta z$. Behind the scenes, the solver determines the maximum step Δz possible on a global scale, since some parts of the grid may contain finer features, and require shorter integration steps than others. Unlike the fully spectral UPPE, the length of the integration step the ODE solver is permitted to take is bounded from above by the maximum step allowed by the BPM method used for the linear propagator.

(2) *Re-align the spectral amplitudes*. The point along z at which A and E amplitudes coincide can, of course, be chosen arbitrarily. It is advantageous to renew this synchronization point after each ODE step such that A and E coincide at the beginning of the ODE step. This is achieved by

$$A_{\perp}^{F} \leftarrow e^{+i\sqrt{\hat{L}}\Delta z} A_{\perp}^{F}, \tag{49}$$

which amounts to yet another application of the linear-problem propagator to the current solution. Naturally, Δz must be obtained from the ODE solver as the actual length of the last adaptive integration step. This repeated re-alignment step is normally implemented in bulk-media UPPE solvers as well. In that case, however, implementations without it are possible, in principle. Here, it is crucial that the step length in the linear propagator is kept small, and application of Eq. (49) ensures that δz is always smaller than the maximal step allowed in the ODE solver.

In a nutshell, the above procedure describes the standard UPPE solution method modified in two ways: First, a BPM-based propagator is utilized for the (short-step) linear advancement of the optical field, and second, real-space representation of transverse dimensions is retained at all times.

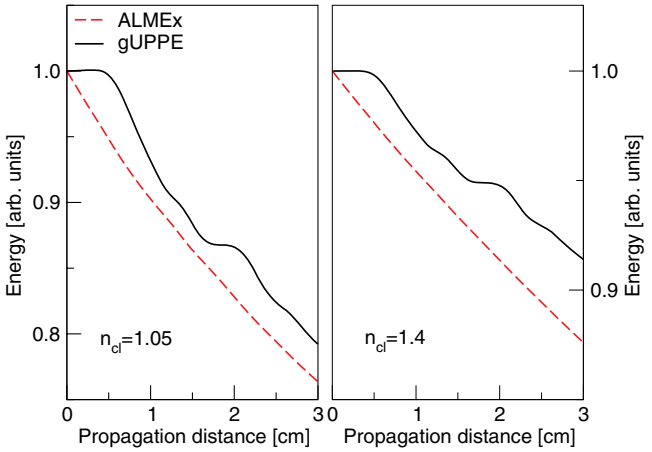

FIG. 1. (Color online) Energy loss experienced by an initially collimated, pulsed Gaussian beam with the beam waist smaller than the capillary inner diameter. The gUPPE approach (solid black line) includes proper modeling of loss due to light leaking into the cladding. The ALMEx method (dashed red line) incorrectly predicts loss vs propagation distance. Left and right panels present results for different values of n_{cl}.

V. NUMERICAL DEMONSTRATION

In this section, an example is presented to demonstrate practical application of the method introduced in this paper. It is motivated by recent experiments with femtosecond filamentation confined to lossy waveguide structures. One example, which is of practical interest for power scaling of self-compressed pulses, utilizes a hollow slab filled with gas that is delimited by two glass plates [38,39]. Another is a capillary filled with a highly pressurized gas, which has been used to generate radiation of extremely high harmonic orders [40]. The common feature of these experiments is that the light dynamics can be characterized by the four attributes (A + B + C + D) we listed in our Introduction. Another common feature is that when such experiments are simulated numerically, the methods are typically based on expansion of the electric field into approximate leaky modes of the corresponding waveguiding structure. Because the femtosecond wave packet is subject to extreme nonlinear dynamics, simulation results are, in general, very sensitive to details of the approximations adopted.

We illustrate the simulation capability of the new generalized unidirectional pulse propagation equation (gUPPE) approach on the case of a pressurized capillary excited by a midinfrared pulse. The parameters we adopt are motivated by recent experiments (see supplementary material for Ref. [40]). We consider a capillary with a 200-μm inner radius, pressurized to 20 atm with argon, and an index of refraction difference n_{cl} between the pressurized core and the waveguide cladding. For simplicity here, we assume constant pressure in the whole volume, although in practice one must also simulate a pressure gradient on the input and output of the waveguide. The input pulse has a wavelength of 3.9 μm and a Gaussian beam profile collimated at the capillary entrance. A beam waist of 100 μm is chosen to avoid exposing the glass cladding to high intensity. The light-gas interaction includes Kerr self-focusing nonlinearity, strong-field and avalanche ionization and corresponding losses, and the defocusing effect of freed electrons described in terms of the Drude plasma model [30].

The numerical approach adopted for this example follows the strategy described in the previous section. We utilize a BPM plugin which implements Eq. (48). From a numerical point of view, the scheme is similar to the well-known Crank-Nicolson method, and we use the corresponding algorithm. To truncate the computational domain in the transverse direction, our BPM plugin uses a perfectly matched layer (PML) as the absorbing boundary condition.

It is illustrative to start with a purely linear case that elucidates why the usual method of approximate leaky mode expansion (ALMEx) may fail in situations with higher order modes excited. Figure 1 shows energy loss as a function of propagation distance inside a capillary computed with the gUPPE method and the standard ALMEx approach. Since the beam waist of the pulse on entrance to the waveguide is smaller than the capillary bore, losses due to light leaking into the capillary cladding are initially very small. This is correctly reflected in the gUPPE model. Moreover, under propagation, the pulse is spatially reshaped. The nearly horizontal sections of the gUPPE curves occur when the pulsed beam barely touches the glass-gas interface and leakage is reduced. In contrast, the ALMEx method predicts immediate loss, despite the fact that the beam is not in contact with the glass interface. This is because the losses in ALMEx are based on complex-valued propagation constants ascribed to an orthonormal set of modes. Consequently, the energy of the wave packet is the sum of modal energies, and the total energy decrease is always at least as fast as that of the fundamental mode. In other words, the leakage losses do not depend on the transverse shape of the beam inside the hollow waveguide. In order to show that the relative error in capturing the loss remains comparably the same, independent of the overall waveguide loss, we present two examples with different refractive indices of the cladding n_{cl}. Note that for the realistic case, in which the loss is smaller,

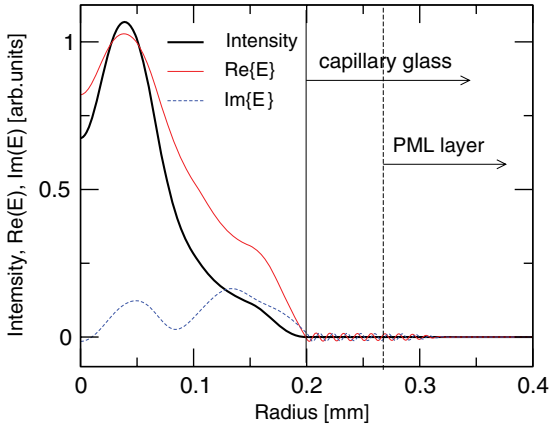

FIG. 2. (Color online) An example of the spatial profile of the optical field (taken at the central time slice $\tau = 0$ of the pulse) after propagation in the nonlinear regime. The dip in the center is caused by defocusing due to electrons freed by the leading edge of the pulse. The light leaking into the cladding is evident beyond $r = 200$ μm, as is the damping in the PML. The grid used to sample the radial dimension was chosen equidistant, with 800 points over 0.4 mm total radius. The propagation distance of this snapshot is $z = 1.5$ cm.

the relative error in overestimating loss is actually greater. These issues and their consequences will be discussed in detail elsewhere.

We next consider the fully nonlinear regime with the proposed gUPPE framework by simulating the propagation of a pulse, with a high initial intensity of 10^{18} W/m^2, through 4 cm of a hollow capillary waveguide. The nonlinear dynamics results in complete spatial and temporal reshaping of the wave packet (Figs. 2 and 3). It is evident from the fine features in Fig. 3 that in addition to low-order leaky modes, higher order modes get significantly excited. If a superposition is created with sharp spatial structures (such as those due to self-focusing) localized in the capillary center, the ALMEx method will introduce unphysical loss that artificially dampens such nonlinear events. Figure 4 illustrates extreme spectral broadening. Although it is a common occurrence in nonlinear

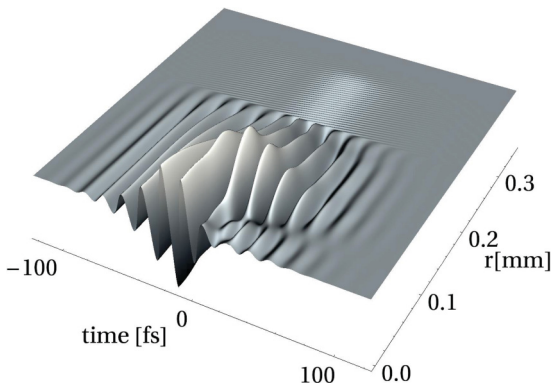

FIG. 3. (Color online) Spatiotemporal reshaping of a midinfrared pulse in a hollow capillary waveguide. The trailing edge of the pulse in the on-axis region is depleted due to generated plasma. The diagonal texture visible for $r > 200$ μm is the outgoing radiation eventually absorbed in the PML. The propagation distance of this snapshot is $z = 0.5$ cm.

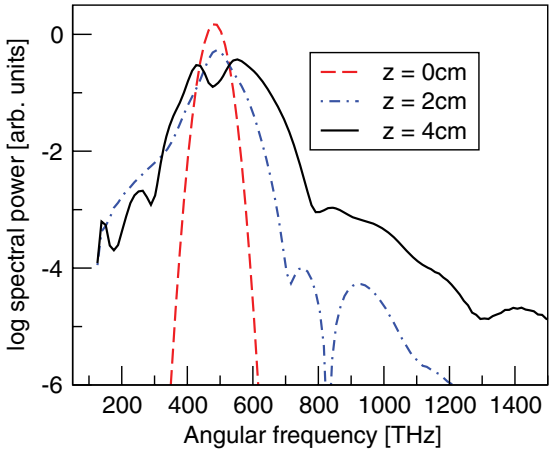

FIG. 4. (Color online) Extreme spectral broadening (supercontinuum). The propagation regime in the hollow waveguide at high pressure is akin to femtosecond filamentation with the concomitant supercontinuum generation reflecting the extreme nonlinear evolution.

regimes, methods restricted to a single frequency (or narrow range), like BPM, fail to capture the physics. Taking all of these results together, the gUPPE method is seen to successfully simulate situations with all four of the attributes discussed in the Introduction.

Naturally, numerical simulation of such rich dynamic evolution requires considerable computational resources. However, the gUPPE approach performs comparably to ALMEx in terms of the compute time required, because in both methods, nonlinearity forces the integration step to be submicron. Although the BPM-based linear propagators (one for each angular frequency resolved) do require a larger grid, they are implemented using a proven and efficient algorithm which scales linearly with the number of grid points. On the other hand, the spectral method underlying ALMEx slows down quadratically with increasing resolution, and requires a full-matrix spectral transform. As a result, the gUPPE method is not only a better, more realistic model, but is also competitive in terms of performance [41].

VI. SUMMARY

We have presented a generalization of the unidirectional pulse propagation equation suitable for structures characterized by material interfaces parallel to the pulse propagation direction and by strong differences between the properties of the constituent materials. While the main result of Eq. (40) is somewhat intuitive, we show a rigorous derivation based on identification of the forward and backward propagating wave components. These are expressed in terms of projection operators [Eqs. (27) and (28)] akin to those we have previously used in bulk media [12]. They allow expression of the generalized UPPE in terms of the linear propagator, and they "isolate" the nonlinear interactions with the medium, such that the evolution is described in terms of spectral amplitudes which only evolve due to nonzero nonlinearity.

The generalized UPPE uses a mixed representation: spectral for the frequency (time) dimension and real space for

the transverse (to the direction of propagation) dimensions. The linear propagator can be based on one of the many available beam-propagation methods. The concrete choice of the method will depend on the given geometry. For example, the pressurized capillary considered in this paper was treated using a radial WA-BPM with a PML boundary to absorb leaking radiation. Independent of the chosen BPM approach, the numerical solution strategy developed previously for bulk-media UPPEs can be used with relatively minor modifications. Our illustrations show that extreme nonlinear dynamics can be efficiently simulated, having compute times comparable to more typical algorithms.

Let us also note that we have dealt with the so-called z-propagated version of pulse propagation equations. Similar formulation is possible also for its counterpart, in which the evolution is integrated along the temporal axis (t-propagated equations). On the one hand, this requires additional assumptions to be able to calculate nonlinear responses [30], but on the other hand it simplifies calculation of the longitudinal field components. It could therefore be of practical interest to also explore such t-propagated versions of this method.

There is an increasing interest in extreme nonlinear optics confined to waveguiding structures of different kinds. It is therefore expected that our results will find application in various implementations of efficient pulse propagation solvers, especially situations in which both the geometry of the structure and waveform reshaping due to nonlinear interactions play important roles.

ACKNOWLEDGMENT

This work was supported by the US Air Force Office for Scientific Research under Grant No. FA9550-11-1-0144.

[1] J. V. Roey, J. van der Donk, and P. E. Lagasse, J. Opt. Soc. Am. **71**, 803 (1981).
[2] Y. Chung and N. Dagli, IEEE J. Quantum Electron. **26**, 1335 (1990).
[3] H. Rao, R. Scarmozzino, and J. R. M. Osgood, IEEE Photon. Technol. Lett. **11**, 830 (1999).
[4] R. Scarmozzino, A. Gopinath, R. Pregla, and S. Helfert, IEEE J. Sel. Top. Quantum Electron. **6**, 150 (2000).
[5] K. Saitoh and M. Koshiba, IEEE J. Quantum Electron. **38**, 927 (2002).
[6] S. T. Hendow and S. A. Shakir, Appl. Opt. **25**, 1759 (1986).
[7] J. Shibayama, M. Muraki, J. Yamauchi, and H. Nakano, J. Lightwave Technol. **23**, 2285 (2005).
[8] H. M. Masoudi and M. S. Akond, J. Lightwave Technol. **29**, 2475 (2011).
[9] A. Taflove and S. Hagness, *Computational Electrodynamics*, 3rd ed. (Artech House, Boston, 2005).
[10] J. H. Greene and A. Taflove, Opt. Express **14**, 8305 (2006).
[11] H. Schmitz and V. Mezentsev, J. Opt. Soc. Am. B **29**, 1208 (2012).
[12] M. Kolesik, J. V. Moloney, and M. Mlejnek, Phys. Rev. Lett. **89**, 283902 (2002).
[13] M. Kolesik and J. V. Moloney, Phys. Rev. E **70**, 036604 (2004).
[14] T. Brabec and F. Krausz, Phys. Rev. Lett. **78**, 3282 (1997).
[15] B. Crosignani, P. Di Porto, and A. Yariv, Opt. Lett. **22**, 778 (1997).
[16] M. Trippenbach and Y. B. Band, Phys. Rev. A **56**, 4242 (1997).
[17] M. Trippenbach and Y. B. Band, Phys. Rev. A **57**, 4791 (1998).
[18] M. Geissler, G. Tempea, A. Scrinzi, M. Schnürer, F. Krausz, and T. Brabec, Phys. Rev. Lett. **83**, 2930 (1999).
[19] M. A. Porras, Phys. Rev. A **60**, 5069 (1999).
[20] A. V. Husakou and J. Herrmann, Phys. Rev. Lett. **87**, 203901 (2001).
[21] P. Kinsler and G. H. C. New, Phys. Rev. A **67**, 023813 (2003).
[22] P. Kinsler, S. B. P. Radnor, and G. H. C. New, Phys. Rev. A **72**, 063807 (2005).
[23] P. Kinsler, Phys. Rev. A **81**, 013819 (2010).
[24] S. Chen, A. Jarnac, A. Houard, Y. Liu, C. L. Arnold, B. Zhou, B. Forestier, B. Prade, and A. Mysyrowicz, J. Opt. Soc. Am. B **28**, 1009 (2011).
[25] M. A. Foster, A. C. Turner, M. Lipson, and A. L. Gaeta, Opt. Express **16**, 1300 (2008).
[26] M. R. E. Lamont, B. Luther-Davies, D.-Y. Choi, S. Madden, and B. J. Eggleton, Opt. Express **16**, 14938 (2008).
[27] R. Halir, Y. Okawachi, J. S. Levy, M. A. Foster, M. Lipson, and A. L. Gaeta, Opt. Lett. **37**, 1685 (2012).
[28] P. Kinsler, J. Opt. Soc. Am. B **24**, 2363 (2007).
[29] P. Kinsler, Phys. Rev. A **81**, 023808 (2010).
[30] A. Couairon, E. Brambilla, T. Corti, D. Majus, O. d. J. Ramírez-Góngora, and M. Kolesik, Eur. Phys. J. Special Topics **199**, 5 (2011).
[31] G. R. Hadley, Opt. Lett. **17**, 1426 (1992).
[32] G. R. Hadley, Opt. Lett. **17**, 1743 (1992).
[33] Y. Y. Lu and P. L. Ho, Opt. Lett. **27**, 683 (2002).
[34] K. Q. Le and P. Bienstman, J. Opt. Soc. Am. B **26**, 353 (2009).
[35] M. Kolesik, P. T. Whalen, and J. V. Moloney, IEEE J. Sel. Top. Quantum Electron. **18**, 494 (2012).
[36] A. Couairon and A. Mysyrowicz, Phys. Rep. **441**, 47 (2007).
[37] L. Bergé, S. Skupin, R. Nuter, J. Kasparian, and J.-P. Wolf, Rep. Prog. Phys. **70**, 1633 (2007).
[38] S. Akturk, C. L. Arnold, B. Zhou, and A. Mysyrowicz, Opt. Lett. **34**, 1462 (2009).
[39] C. L. Arnold, S. Akturk, M. Franco, A. Couairon, and A. Mysyrowicz, Opt. Express **17**, 11122 (2009).
[40] T. Popmintchev, M.-C. Chen, D. Popmintchev, P. Arpin, S. Brown, S. Alisauskas, G. Andriukaitis, T. Balciunas, O. D. Mücke, A. Pugzyls *et al.*, Science **336**, 1287 (2012).
[41] gUPPE provides a general framework to implement nonlinear pulse propagation solvers in nontrivial waveguiding structures, but the optimal choice of BPM plugin for the linear propagators depends on the context.